Numerical modeling of turbulent convection and acoustic wave propagation in the solar interior

By M. S. Miesch†, N. N. Mansour AND M. M. Rogers

The advent of helioseismology and the increasing sophistication of numerical models have brought forth a new era in our understanding of solar interior dynamics. High-resolution simulations of turbulent convection have become essential tools in the interpretation of helioseismic data and have provided new insight into the maintenance of large-scale flows and magnetic fields in the solar interior. Still, we can do better. One of the largest uncertainties in current numerical models is the influence of the upper and lower boundary regions which surround the convective envelope and which cannot be fully resolved in a global simulation. In this summer school we began to investigate in more detail the sensitivity of convection simulations to these boundary regions and we found that they have a more significant impact than might be supposed. We also initiated an investigation into the propagation of acoustic waves in the solar interior and their interaction with flow fields, thermal inhomogeneities, and magnetic structures. This project promises to elucidate the *forward problem* of helioseismology, providing essential theoretical support to ongoing observational efforts.

1. Introduction

The sun acts as a resonant cavity. Like a bell with millions of distinct tones, the sun rings with global acoustic oscillations. By studying subtle variations in the frequencies of these oscillations, solar physicists have begun to infer something about the structure and dynamics below the solar photosphere. This is the science of helioseismology, and in the past few decades it has revolutionized the study of solar interior dynamics. This is an exciting time to be a solar physicist.

From a dynamical perspective, the most profound achievement of helioseismology has been the mapping of the internal rotation profile of the sun as a function of latitude and radius. The sun does not rotate as a solid body. Rather, it rotates differentially, with a rotational period of about 25 days near the equator and about 34 days near the poles. The surprise from helioseismology is that this monotonic decrease of angular velocity by about 30% from equator to pole is approximately independent of radius throughout the convection zone (Thompson *et al.* 2003). Below the convection zone, the rotation appears to be uniform within the errors of the helioseismic inversions. The transition from differential to uniform rotation occurs across a narrow region of strong rotational shear located near the base of the convection zone, which has been named the solar tachocline.

Keeping pace with the dramatic progress of helioseismic investigations, dynamical models of the solar interior are becoming increasingly sophisticated. High-resolution numerical simulations have given us new insight into the nature of the solar convection

† HAO/NCAR, Boulder, CO 80307-3000 (The National Center for Atmospheric Research is sponsored by the National Science Foundation)

zone, which occupies the outer 30% of the solar interior by radius and which is thought to be highly turbulent, with Reynolds numbers exceeding 10^{12}.

One such numerical model is based on the ASH (Anelastic Spherical Harmonic) code, which was developed at the University of Colorado and JILA (Clune *et al.* 1999). The first scientific results were reported by Miesch *et al.* (2000) and since then, much progress has been made in further developing the model and in exploring different parameter regimes, different geometries, and different physical processes (Miesch 2000; Elliot, Miesch & Toomre 2000; Brun & Toomre 2002; DeRosa, Gilman, & Toomre 2002; Brun, Miesch & Toomre 2004).

Despite the success that the ASH code has enjoyed, further model development is always warranted in a system as complex as the sun. One of the primary questions that is still poorly understood is what effect the convection zone boundary regions have on the global dynamics. At the bottom of the convection zone there is a stiff transition from sub-adiabatic to super-adiabatic stratification, giving rise to a narrow region of convective overshoot. Meanwhile, at the top of the convection zone, there is a complex transition between the envelope where heat is carried outward by convection and the relatively sparse corona where the heat transport is dominated by radiation. Radiative transfer effects, coupled with the steep sub-surface stratification and the ionization of hydrogen, drives vigorous convective motions known as granulation.

The main difficulty with these boundary regions is their relatively small scale. Differential rotation occurs on global scales of $\sim$ 1000 Mm and requires the full spherical geometry to properly address. It is thought to be maintained by large-scale convective motions which are driven by buoyancy on scales of perhaps a few hundred Mm. Granulation, by comparison, occurs on scales of a few Mm, well beyond the resolution of even the most ambitious global-scale model. Furthermore, the overshoot region at the base of the convection zone is no more than 10 Mm thick–less than 1% of the solar radius. Global models cannot accurately capture the complex, small-scale dynamics occurring in these interface regions so some approximations are necessary.

In this summer school we focused on two primary objectives. The first was to investigate in more detail the sensitivity of global solar convection simulations to the upper and lower boundary conditions. We already know that in a global model we cannot explicitly resolve the complex dynamics which occur in the upper and lower transition regions bordering the solar convection zone. What we wish to understand better is: what difference does this make? How sensitive are global features such as the differential rotation to what occurs in the boundary layers?

Our second objective in this summer school was to begin to investigate in greater detail the coupling between large-scale convection and the acoustic waves, known as p-modes, which form the basis of helioseismology. Large-scale convection does not generate p-modes; it's Mach number is too low to be a significant source of acoustic power. Rather, p-modes are generated in the near-surface layers by granulation and propagate downward throughout the convection zone and deep interior.

Although p-modes do not significantly influence the dynamics of large-scale convection, they are the primary diagnostic tool used to probe such motions. Helioseismic inversions rely on p-modes to infer flow fields and structural information about the solar interior. Thus, it is of great practical importance to understand how acoustic waves interact with convective motions and other dynamical phenomena such as zonal jets and magnetic flux tubes.

Since it makes use of the anelastic approximation, the ASH code cannot be used to

	lower boundary	upper boundary
Case A	penetrative	moderate entropy gradient
Case B	non-penetrative	moderate entropy gradient
Case C	non-penetrative	large entropy gradient

TABLE 1. Simulation Summary

follow the propagation of acoustic waves (see §3). Thus, we have developed a separate acoustic solver which will eventually piggyback on the ASH code. However, before we address the acoustic probing of turbulent convection, which is a formidable problem, we will first consider the interaction between a specified acoustic wave field and simple inhomogeneities such as Gaussian temperature perturbations, smooth meridional circulations, and localized zonal jets and magnetic flux tubes.

In the sections that follow, we will say a few more words about each of these projects in turn and where they may be heading.

2. Boundary Sensitivities

The simulations we will describe are carried out using the ASH code, which solves the 3D equations of fluid motion in a rotating spherical shell (Clune *et al.* 1999). The ASH code is based on the anelastic approximation, which is designed for substantially subsonic motions in the presence of a background density stratification. The equations are solved using a pseudo-spectral technique, with spherical harmonic basis functions in the horizontal directions and a stacked Chebyshev expansion in the vertical. Time-stepping is accomplished with an explicit Adams-Bashforth scheme for the nonlinear terms and a semi-implicit Crank-Nicolson scheme for the remaining linear terms. The boundary conditions used here are impenetrable and stress-free, with a fixed entropy gradient. In the applications presented here we neglect magnetic fields.

In order to investigate the sensitivity of global-scale solar convection to the imposed boundary conditions, we have initiated a series of simulations, three of which are summarized in Table 1. Case B can be viewed as the *control* simulation. This case is non-penetrative, meaning that the impenetrable lower boundary of the computational domain is placed at the base of the convection zone, at $r \approx 0.7R_\odot$. By contrast, in Case A, the lower boundary of the computational domain is placed well below the base of the convection zone, at $r = 0.55R_\odot$. Thus, Case A allows penetration into a stably stratified region below the convective envelope.

The third simulation we describe here, case C, is similar to case B, but we have imposed a larger entropy gradient on the upper boundary, as suggested by some 1D solar structure models (e.g. Christensen-Dalsgaard *et al.* 1996). The difference between the entropy gradient in cases B and C is illustrated in Figure 1a. Each simulation begins with a monotonic decrease in the entropy gradient from its surface value to the lower value imposed at the bottom boundary. However, in all cases, redistribution of entropy by convective motions produces a local minimum in the entropy gradient just below the surface. The entropy gradient in case A is similar to that in case B except that it increases sharply to 10^{-4} below the base of the convection zone at $r = 0.71R_\odot$.

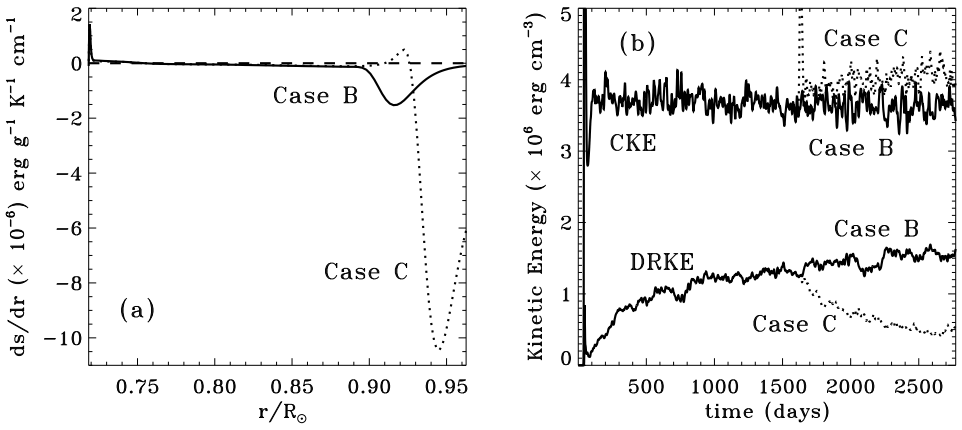

FIGURE 1. Frame (a) shows the horizontally averaged radial entropy gradient in case B (solid line) and case C (dotted line) late in the simulations (t = 2770 days and t = 2860 days, respectively). In frame (b), the volume-averaged convection kinetic energy (upper curves) and differential rotation kinetic energy (lower curves) are plotted as a function of time for case B (solid lines) and case C (dotted lines).

Cases A and B were initiated from static initial conditions, but case C was restarted from case B after the latter had evolved for about 1600 days. Figure 1b shows the time evolution of the kinetic energy contained in the non-axisymmetric convective motions (CKE) and the kinetic energy contained in the differential rotation (DRKE), both relative to a rotating coordinate system for cases B and C. The convection kinetic energy in case B saturates quickly, reaching a statistically steady state within about 100 days. By contrast, the differential rotation for the same case takes a much longer time to establish and is still growing slowly after about 2000 days.

After the simulation is continued with a different upper boundary condition (case C), the convective kinetic energy increases slightly because of stronger driving in the upper boundary layer. Surprisingly, the change in boundary conditions has also produced a substantial drop in the differential rotation kinetic energy. This decrease is apparent in the differential rotation profiles shown in Figure 2.

Figure 2 indicates that the latitudinal angular velocity variations in cases A and C are both much smaller than in case B. This implies that the presence of an overshoot region and stronger driving near the top of the shell both tend to decrease the differential rotation in the bulk of the convection zone, at least in the parameter regimes studied here. The former conclusion is only tentative, however, because case A has only been evolved for a few hundred days and may not have had time to establish a steady rotation profile. The angular velocity contrast in the sun between the equator and high latitudes is about 30%, somewhat more than that in case B. Thus, the smaller angular velocity gradients in cases A and C are not solar-like.

Despite the divergent rotation profiles in the three simulations, the convection patterns appear similar as shown in Figure 3. The biggest difference occurs with case C, in which the downflow lanes appear relatively narrow and the convection network somewhat more isotropic. This can again be attributed to the stronger buoyancy driving near the surface.

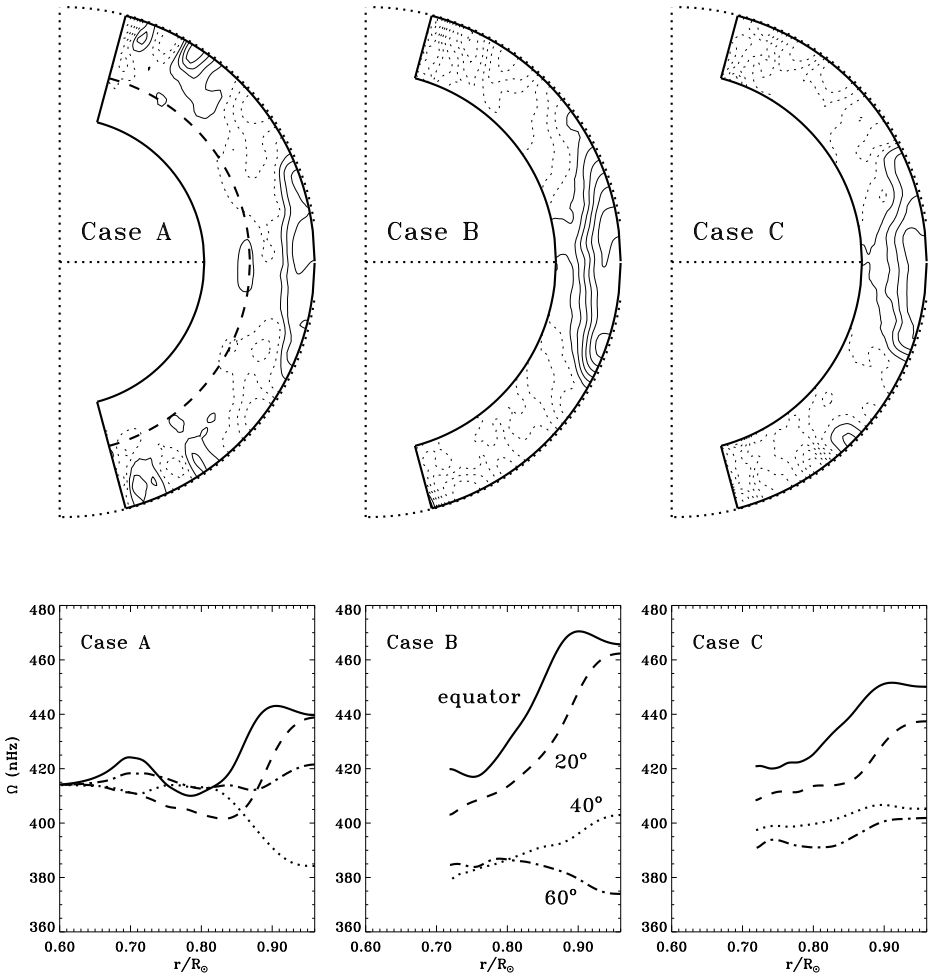

FIGURE 2. The upper frames show the longitudinally averaged angular velocity profile in cases A, B, and C at a time late in the evolution of each simulation. The dashed line in Case A indicates the base of the convection zone. Corresponding radial cuts at chosen latitudes (averaged over both hemispheres) are shown in the lower frames. The polar regions are not shown because there the moment arm, $r\sin\theta$ (θ being the co-latitude) approaches zero and the angular velocity is not well defined.

3. Acoustic Wave Propagation

As mentioned in §1, our primary means of probing solar interior dynamics is through acoustic waves, which are analyzed using the techniques of helioseismology. At the heart of this endeavor lies the so-called *forward problem*; for a given flow or field structure, what acoustic signal will be manifested in the photosphere, where we can observe it?

The influence of flow fields and related structural or magnetic variations on acoustic mode propagation depends on the nature of the modes. For global, resonant oscillations

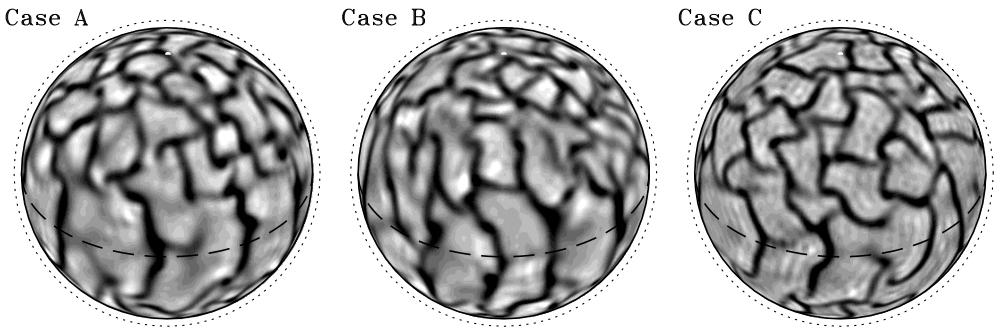

FIGURE 3. Snapshots of the radial velocity field are shown for cases A, B, and C at a horizontal layer near the top of the shell. In these grayscale images, upflows appear bright and downflows appear dark. Each image is an orthographic projection with the north pole tilted 30° toward the observer. The dotted line indicates the outer boundary of the computational domain and the dashed line indicates the equator.

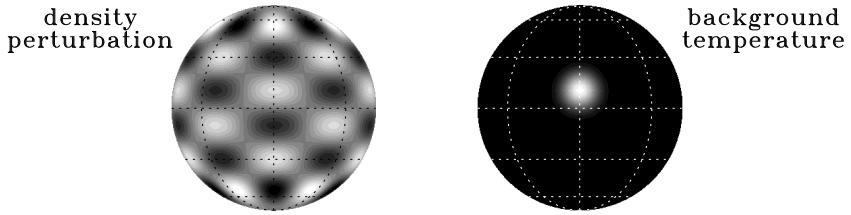

FIGURE 4. Initial conditions for one of our acoustic wave simulations. The density perturbation is chosen to be a spherical harmonic mode with $\ell = 10$, $m = 5$, propagating eastward (toward the right) at a rate equal to the sound speed. The background temperature is uniform except for a Gaussian enhancement (by a factor of two) located at a latitude of 10° N and a longitude of 0°.

of the entire sphere, dynamical variations are manifested as shifts in the oscillation frequencies. Although relatively straightforward to calculate, these shifts can be subtle and difficult to detect. Furthermore, different dynamical processes can give rise to similar frequency shifts, so even if a shift is detected, it may be difficult to interpret. For a local spectrum of high-wavenumber traveling waves the forward problem becomes even more complicated. In both the global and local cases, numerical simulations can potentially provide much new insight.

Over the course of this summer school, we have initiated a project to investigate the interaction between acoustic wave fields and inhomogeneities induced by convective flows or other dynamical processes (e.g. magneto-rotational instabilities in the tachocline). We have developed a numerical model that uses much of the machinery already implemented in the ASH code, such as spherical harmonic transforms and radial derivatives. However, the ASH code is based on the anelastic approximation, which effectively filters out acoustic waves because the time derivative in the mass continuity equation is neglected ($\boldsymbol{\nabla}\cdot(\overline{\rho}\mathbf{v}) = 0$, where $\overline{\rho}$ is the background density). Therefore, we have developed a distinct set of equations designed to follow the propagation of linear, inviscid acoustic waves in a background medium that may in general possess flows and inhomogeneities in the sound speed.

The acoustic equations are derived from the equations of mass and momentum conser-

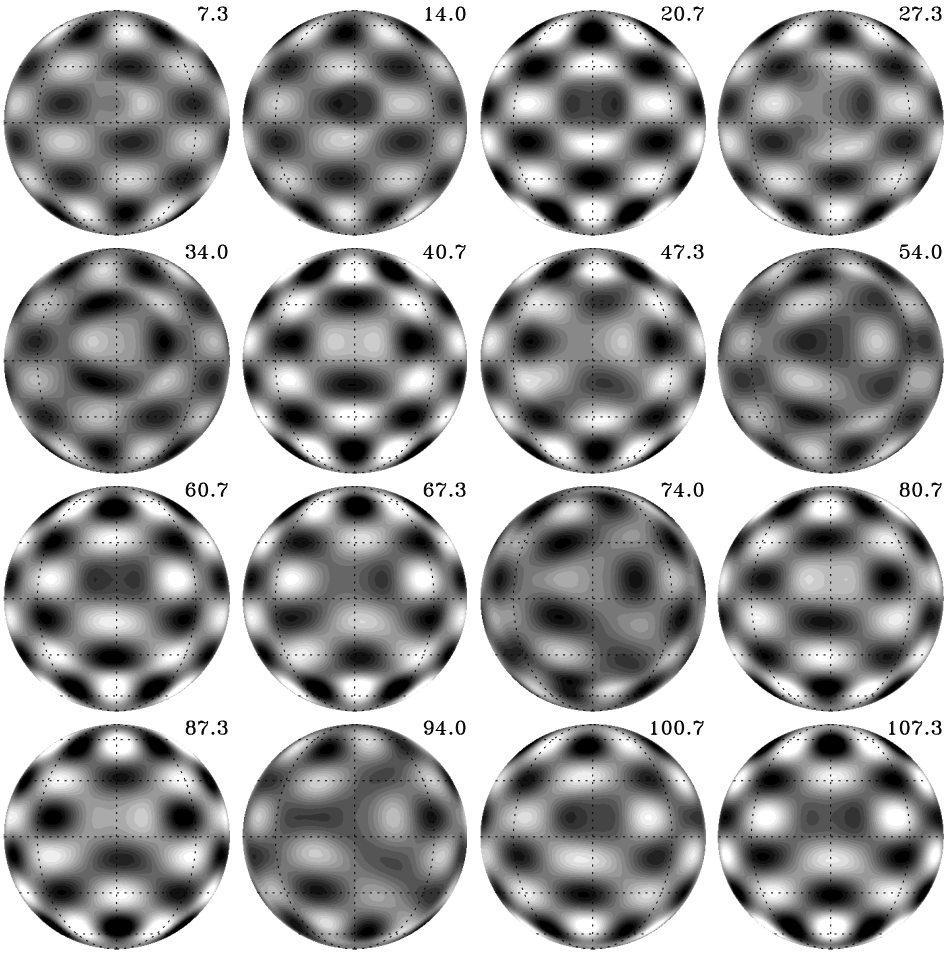

FIGURE 5. The density field is shown as the simulation evolves. As in Figure 4, bright areas denote density enhancements and dark areas rarefactions. The time (in minutes) is indicated to the upper right of each frame. The interval between frames is 400 seconds (6.66 min).

vation for a compressible fluid. As a first approximation we consider adiabatic acoustic waves, but as the project proceeds we will incorporate thermal diffusion, buoyancy, and rotation. With regard to the background state, we will start simple and build up to more complex configurations. Thus, the background state, indicated by an overbar, is for now assumed to be static: $\overline{\mathbf{v}} = 0$. The equations for mass continuity and momentum conservation then reduce to

$$\frac{\partial \rho'}{\partial t} + \boldsymbol{\nabla}^2 \varphi = 0 \tag{3.1}$$

and

$$\frac{\partial}{\partial t} \boldsymbol{\nabla}^2 \varphi + \boldsymbol{\nabla}^2 \left(c_s^2 \rho' \right) = 0 \quad , \tag{3.2}$$

where ρ' is the perturbation density, c_s is the sound speed, and φ is the velocity potential,

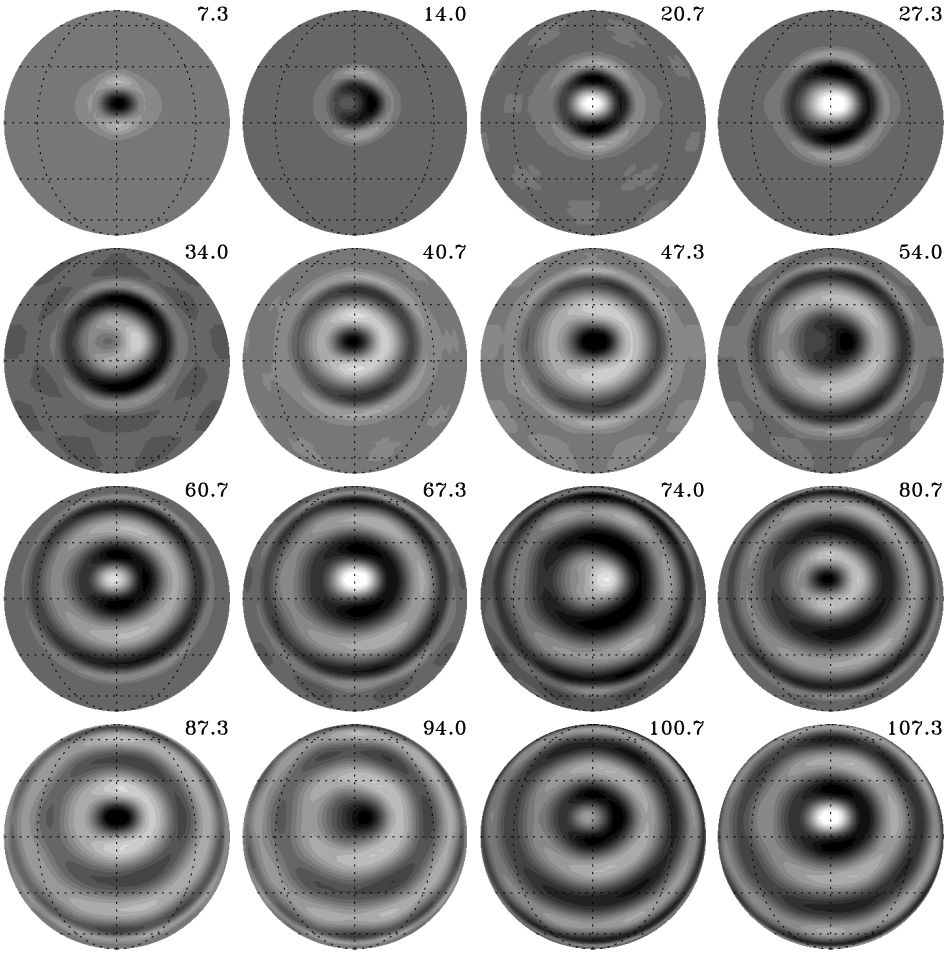

FIGURE 6. Similar to Figure 5 but with the $\ell = 10$, $m = 5$ component subtracted out.

defined in terms of the perturbation mass flux $\mathbf{m}'$ as

$$\mathbf{m}' = \boldsymbol{\nabla}\varphi + \boldsymbol{\nabla}\times\boldsymbol{\Psi} \quad . \tag{3.3}$$

The incompressible component of the velocity field, represented by the vector streamfunction $\boldsymbol{\Psi}$, does not enter into the acoustic equations. For an ideal gas, the sound speed $c_s = \sqrt{C_P(\gamma-1)\overline{T}}$, where C_p is the specific heat at constant pressure, γ is the ratio of specific heats, and $\overline{T}$ is the background temperature.

We solve equations (3.1)–(3.2) using a pseudo-spectral technique with spherical harmonic basis functions and a leap-frog temporal differencing scheme. One of our first test cases is illustrated in Figures 4–6. As a starting point we consider a 2–D spherical surface and we initialize our system with a specified density perturbation represented by the spherical harmonic mode of degree $\ell = 10$ and order $m = 5$ (Figure 4). The initial velocity potential is given a similar structure but with a phase lag appropriate for an

eastward-propagating wave. Thus, if the background sound speed is homogeneous, the "soccer ball" pattern in the left frame of Figure 4 will simply propagate to the right, maintaining its spatial structure indefinitely.

We now introduce an inhomogeneity. The background temperature field is given a local enhancement centered at a latitude of 10°N and a longitude of 0° as shown in the right frame of Figure 4. The form of the enhancement is Gaussian, with an e-folding length of 10° and a peak value which is twice the background temperature. Thus, the local sound speed is increased by a factor of $\sqrt{2} = 1.4$. This can be regarded as a crude (and exaggerated) first approximation to a sunspot or active region, which are generally associated with localized thermal variations.

The evolution of the simulation is illustrated in Figure 5. The eastward-propagating acoustic wave scatters off the temperature enhancement, sending out a series of circular acoustic pulses. The distortion of the acoustic mode is apparent, but the density field is still dominated by the $\ell = 10$, $m = 5$ mode, which was imposed as the initial condition and which drives the dynamics.

The structure of the acoustic pulses can be seen more clearly if we subtract out the primary driving mode as shown in Figure 6. The temperature enhancement acts as a scattering center, sending off divergent circular waves with a continually varying phase. These waves extract energy from the primary mode, eventually causing it to decay.

4. Conclusions and Outlook

The results presented here are preliminary. Both projects described in sections 2 and 3 are ongoing and there is much work to be done. First, it must be verified that the patterns identified in §3 are robust, particularly with regard to the differential rotation. The existing cases must be evolved for longer durations in order to confirm that the rotation profiles are indeed steady and new cases must be initiated in order to make sure that our conclusions are not limited to the particular parameter regimes chosen here.

Another boundary condition that we plan to investigate was motivated in part by discussions we had with Profs. Nordlund and Stein during the summer school. According to their simulations of granulation in the solar surface layers, motions that possess a non-zero horizontal divergence tend to deform the outer surface rather than turn over upon themselves. Thus, to lowest order, the horizontal divergence is approximately independent of depth, implying a small vertical divergence of the mass flux: $\partial(r^2\overline{\rho}v_r)/\partial r \approx 0$. We have used this result to devise open boundary conditions for the top of our domain that allow flow through the boundary. Since our outer boundary lies within the solar convection zone, this promises to be a more realistic treatment of the upper boundary, provided that it is numerically stable. We implemented this new boundary condition during the summer school but have not yet fully tested it.

With regard to the acoustic wave investigations, the results shown here are only the beginning. Our next step is to add the radial dimension to our acoustic solver and to implement boundary conditions which are realistic and useful from the point of view of helioseismology. We must then incorporate thermal diffusion, buoyancy, and rotation into our formulation. Once these code developments are finished, we will be prepared to investigate the interaction between an acoustic wave field and a series of imposed flows and structural variations of progressively increasing complexity. We will begin by studying the response of an imposed spectrum of acoustic waves to thermal inhomogeneities such as the Gaussian enhancement considered here. The results will be interpreted in

a helioseismic context and applied to practical problems such as far-side imaging. We will then investigate the acoustic signatures of flow variations such as zonal jets and meridional circulations. Eventually we will study these same problems and more in the presence of an evolving, convective, background flow computed with the ASH code.

We thank Juri Toomre and Sacha Brun for taking part in our continuing adventures with the ASH code. We appreciate their insight and support. We also thank Sasha Kosovichev for motivating much of the work initiated here and Aake Nordlund, Bob Stein, and Freidrich Busse for simulating discussions during the summer school. Mausumi Dikpati reviewed this manuscript for NCAR and we thank her for her comments. MSM would also like to thank Parviz Moin, Nagi Mansour, and their colleagues at CTR for an inspiring and productive program.

REFERENCES

Brun, A. S., Miesch, M. S. & Toomre, J. 2004 Global-Scale Turbulent Convection and Magnetic Dynamo Action in the Solar Envelope. *Astrophys. J.* (in press)

Brun, A. S. & Toomre, J. 2002 Turbulent Convection under the Influence of Rotation: Sustaining a Strong Differential Rotation. *Astrophys. J.* **570**, 865-885.

Christensen-Dalsgaard et al. 1996 The Current State of Solar Modeling. *Science* **272**, 1286-1291.

Clune, T. C., Elliott, J. R., Miesch, M. S., Toomre, J. & Glatzmaier, G. A. 1999 Computational Aspects of a Code to Study Rotating Turbulent Convection in Spherical Shells. *Parallel Comput.* **25**, 361-380.

DeRosa, M. L., Gilman, P. A. & Toomre, J. 2002 Solar Multiscale Convection and Rotation Gradients Studied in Shallow Spherical Shells. *Astrophys. J.* **581**, 1356-1374.

Elliott, J. R., Miesch, M. S. & Toomre, J. 2000 Turbulent Solar Convection and its Coupling with Rotation: The Effect of Prandtl Number and Thermal Boundary Conditions on the Resulting Differential Rotation. *Astrophys. J.* **533**, 546-556.

Miesch, M. S. 2000 The Coupling of Solar Convection and Rotation. *Solar Phys.* **192**, 59-89.

Miesch, M. S., Elliott, J. R., Toomre, J., Clune, T. C., Glatzmaier, G. A. & Gilman, P. A. 2000 Three-Dimensional Spherical Simulations of Solar Convection: Differential Rotation and Pattern Evolution Achieved with Laminar and Turbulent States. *Astrophys. J.* **532**, 593-615.

Thompson, M. J., Christensen-Dalsgaard, J., Miesch, M. S. & Toomre, J. 2003 The Internal Rotation of the Sun. *Ann. Rev. Astron. Astrophys.*. **41**, 599-643.